Journal of
Electron Devices
www.jeldev.org

Journal of Electron Devices Vol. 23, Num. 1, 2016, pp 1909-1917

©JED[ISSN:1682 -3427] (print)
©JED[ISSN:1682 -3427] (online)

Effect on structural, morphological, optical and gas sensing behaviour of Cr doped zinc oxide.

Anita Hastir[1*], Nipin Kohli[2], Onkar Singh Kang[3], Virpal[1], Gurpreet Singh[1], Ravi Chand Singh[1]

[1]*Department of Physics, Guru Nanak Dev University, Amritsar-143005, Punjab, India*

[2]*Department of Physics, BBK Dav College for Women, Amritsar-143005, Punjab, India*

[3] *Department of Chemistry, University of Manitoba, Winnipeg, MB R3T 2N2, Canada*

**Corresponding Authors email: anitahastir@gmail.com*

Abstract
In the present work, structural, elemental, optical and gas sensing properties of pure and chromium doped zinc oxide have been studied. Pure and Cr doped ZnO powder was synthesized chemically by co-precipitation route. The concentration of chromium was varied from 0 to 3 wt. % and synthesized samples were characterized by using X-ray diffraction (XRD), Raman spectroscopy, X-ray photoelectron spectroscopy (XPS), field emission scanning electron microscopy (FESEM), transmission electron microscopy (TEM) and UV-Vis spectroscopy techniques. Hexagonal wurtzite crystal structure and oxidation states of elements present in the synthesized samples were determined by XRD and XPS studies respectively. FESEM and TEM micrographs depicted dumbbell shaped morphology of pure zinc oxide and spherical shaped nanoparticles for Cr doped ZnO. Shifting and broadening of Raman peaks with increase in chromium concentration in ZnO samples was observed. UV-Vis spectra exhibited band gap narrowing up to 1wt. % doping and band gap widening for concentration above 1 wt.%. For gas sensing application, thick films of synthesized samples were deposited on alumina substrates. It is found that chromium doped ZnO samples have selectively enhanced the liquefied petroleum gas (LPG) response as compared to other volatile gases. A concentration of 1 wt. % chromium as a dopant gives maximum sensing response for LPG at 300oC as compared to other concentrations. The increase in sensing response with addition of chromium as a dopant in zinc oxide may be attributed to increase in charge carrier concentration, catalytic nature of Cr3+ and lattice disorders.

Keywords: Gas detectors, X-Ray diffraction, Raman Scattering, ZnO.

I. Introduction

THE ease to vary electronic, optical and chemical properties of metal oxide semiconductors makes them prevalent materials for carrying research and making their use. in potential applications such as memory storage devices, gas sensors, solar cell, laser diodes, optoelectronic devices, etc. [1-3]. Metal oxide semiconductors are interesting candidates as gas sensors for detection of toxic, harmful and combustible gases. Among various semiconducting metal oxides, zinc oxide, an n-type semiconductor, is an exciting material to work on as a gas sensor because of its interesting properties such as wide band gap (3.37 eV), large exciton binding energy, good thermal and chemical stability, high electron mobility, occurrence of mesoporous/microporous structures providing high specific surface area and above all its biocompatibility and nontoxic nature [4-6] The significant factors controlling gas sensing behaviour are surface

morphology, specific surface area, defects and disorders, charge carrier concentration etc. [7-9]. It is also believed that gas sensitivity is associated to surface chemical activity and consequently gas sensing applications and catalytic properties should be considered together [10]. Various transition metals, rare earth metals, and noble metals have been used as dopants in zinc oxide in order to modify the above mentioned parameters to enhance the gas sensing properties [11-13]. Qi et al. have found that doping of Indium in ZnO resulted in increase in oxygen vacancies and the no. of electrons which are therefore responsible for high response towards acetone and ethanol as compared to pure ZnO [14]. Kim and co-workers have synthesized Cr doped CuO gas sensor and found variation in morphology and increase in surface area for selective detection of NO2 gas [15]. Sun et al. reported enhanced gas sensing response of Fe doped ordered mesoporous NiO with long range periodicity [16]. Patil and Patil have studied gas sensing properties of surface functionalized ZnO thick films by Cr2O3 obtained by dipping technique [17].

The convenient and widely used approaches by which dopants can be introduced in base material oxides are either surface activation or bulk doping. Surface activation is a coarse method in which doping is not evenly distributed and the exact amount of dopant added on the surface of metal oxide cannot be measured; it is an approximate method while bulk doping involves exact atomic or weight measurements of the dopants to be added. In this work, chromium is used as a bulk dopant because of its low ionization energy as compared to zinc and its high catalytic activity that may result in enhancing the sensitivity of metal oxide gas sensor [18, 19].

In the present study, pure and Cr3+ doped zinc oxide samples have been prepared using a low cost, economical and simple co-precipitation method and their gas sensing property has been investigated. The structural, morphological, elemental and optical properties have been examined and discussed. According to the results obtained, chromium doped zinc oxide samples have selectively enhanced the liquefied petroleum gas (LPG) response as compared to other volatile gases and a concentration optimized at 1wt. % exhibited good sensing response towards LPG. .

II. EXPERIMENTAL DETAILS

A. Preparation of pure and chromium doped zinc oxide powder

All reagents used in the present work were of analytical grade. Zinc acetate dihydrate [$(CH_3COO)_2$ Zn · $2H_2O$], chromium chloride hexahydrate [$CrCl_3 \cdot 6H_2O$] and ammonia were obtained from Loba Chemie, Mumbai, India. Chromium doped zinc oxide powder samples were prepared by using co-precipitation technique. For obtaining zinc oxide sample bearing different chromium concentration, 0.2 M chromium chloride aqueous solution with different concentrations from 0 to 3 wt. % (0, 0.5, 1, 2 and 3 wt.%) was added to various 0.2 M zinc acetate aqueous solutions respectively. To the above samples, ammonium hydroxide was added drop wise at room temperature with continuous stirring to obtain precipitates and the pH of the solution was maintained at pH 8. The precipitates thus obtained were filtered, washed and then dried at 120^{o}C temperature in an oven. The dried powder samples were then calcined at 500^{o}C for three hours.

The samples were named as S0, S0.5, S1, S2 and S3 for 0 (pure), 0.5, 1, 2 and 3 wt. % chromium doped zinc oxide respectively.

B. Material characterization

The prepared samples were characterized by powder X-ray diffraction (XRD) using Cu-Kα radiation with Shimadzu 7000 Diffractometer to determine the crystal structure. Room temperature Raman spectroscopy of as synthesized powder samples was investigated by using Reinshaw inVia micro Raman spectrometer with an argon ion laser at 488 nm excitation wavelength. To determine the elemental composition and the chemical oxidation state of undoped and doped ZnO, X-ray photoelectron spectroscopy measurements were performed in a PHI-5600 instrument using Al Kα monochromatic X-ray source at ambient temperature. Morphological analysis of the synthesized samples was done by using field emission scanning electron microscope (FESEM) with Carl Zeiss SUPRA 55. High resolution transmission electron microscopy was carried out by using JEOL JEM-2100. Optical properties were investigated by Shimadzu UV-2450 spectrophotometer.

C. Sensor fabrication and testing methods

For the fabrication of thick film sensors, the following procedure was employed. About 2 mg of synthesized powder was mixed with few drops of distilled water to form a paste. The paste was then encrusted with the fine brush onto alumina substrate (12 mm×5 mm) having pre-deposited gold electrical contacts (2 mm apart) to obtain a thick film of thickness around 40 μm. Same procedure was adopted to make thick film sensors for pure and chromium doped zinc oxide samples. These thick film samples were dried at room temperature and then heated to 500^{o}C for 30 min in a furnace.

To measure the sensor response of prepared samples, we have employed a home-made apparatus consisting of a potentiometric arrangement, and a 40 L test chamber in which a sample holder, a small temperature controlled oven and a mixing fan were installed. The prepared sensor was placed in a sample holder provided in the test chamber oven at room temperature. The temperature of oven was increased in steps with an interval of 50^{o}C and a fixed amount of gas species was injected into the chamber through a narrow hole provided on top of test chamber. Change in real time voltage signal across a resistance connected in series with sensor was recorded with Keithley

Data Acquisition Module KUSB-3100 connected to a computer reported elsewhere [20]. The sensor response magnitude was determined as Ra/Rg ratio, where Ra and Rg are the resistances of sensor in air ambience and air-gas mixture, respectively.

III. Results and Discussion

A. *XRD analysis*

Figure 1 represents X-ray diffraction pattern of pure and chromium doped zinc oxide powder samples calcined at 500°C. The peaks obtained were compared with standard data which confirmed hexagonal wurtzite structure of zinc oxide (JCPDS 80-0074). From XRD results, it is observed that peaks corresponding to chromium oxide are missing which may be due to low concentration of chromium as a dopant in zinc oxide lattice. A shift in XRD peaks towards higher angle is observed as Cr content is increased up to 1 wt. % (sample S0.5 and S1) which may be attributed to the substitution of larger zinc ions (0.74 Å) with smaller chromium ions (0.63 Å) in the lattice. On increasing Cr content above 1 wt. % (sample S2 and S3), a shift in the position of XRD peaks toward lower angles is noticeable which is interpreted as instigation of Cr dopant at octahedral interstitial sites when Cr content exceeds a certain limit. Similar results have been reported by different authors for Co-doped ZnO films [21], Cr doped ZnO films [22], and Co- doped SnO_2 powder [23].

The shifting in peaks leads to variation in lattice parameters and volume of unit cell. For the hexagonal structure of pure and Cr doped ZnO samples, lattice parameters and volume of unit cell are calculated using equations 1 and 2 respectively.

$$\frac{1}{d^2} = \frac{4}{3}\left(\frac{h^2+hk+k^2}{a^2}\right) + \frac{l^2}{c^2} \quad (1)$$

$$V = 0.866 \times a^2 \times c \quad (2)$$

where a and c represents lattice constant; d is the interplanar spacing ; h, k and l are miller indices and V is the volume of unit cell. The lattice parameters for pure and Cr doped samples have been calculated using (100) and (002) planes. A decrease in lattice parameter 'a' and 'c' is found for sample S0.5 and S1 leading to reduction in interatomic distance thereby resulting in lattice contraction whereas lattice expansion is observed in samples S2 and S3. To determine the bond length of undoped and doped ZnO, following formula has been used [24] as

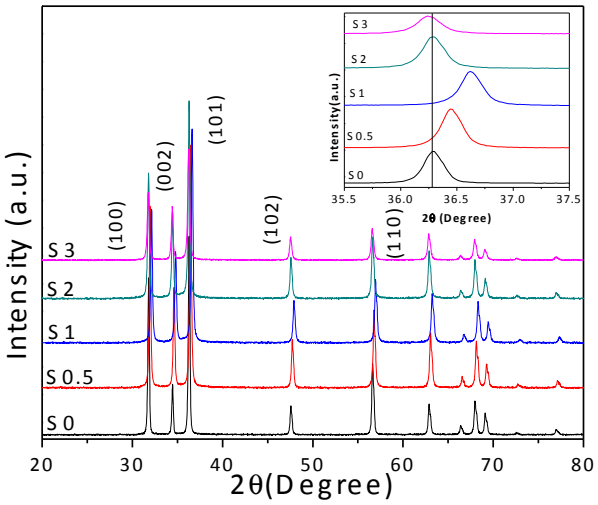

Fig. 1. XRD pattern of pure (S0) and Cr^{3+} doped ZnO (S0.5, S1, S2, S3).

$$L = \sqrt{\frac{a^2}{3} + \left(\frac{1}{2} - u\right)^2 \times c^2} \quad (3)$$

$$u = \frac{a^2}{3c^2} + 0.25 \quad (4)$$

where a and c are lattice parameters and u is a positional parameter.

The crystallite size for the samples has been calculated using Scherrer's formula. The average crystallite size is found to decrease with increase in Cr concentration, because the inclusion of dopant atoms causes distortion in base ZnO lattice reducing the growth rate of crystallite. The calculated crystallite size, lattice parameters, unit cell volume and bond length for sample S0 to S3 are summarized in table 1.

The variations observed in the lattice parameters indeed confirms the substitutional and interstitial incorporation of Cr^{3+} for Zn^{2+} in ZnO creating disorder in ZnO lattice.

TABLE I
Lattice Parameter, Crystallite size (D), Bond Length, Volume of unit cell and Bandgap energies (Eg) of pure and Cr doped ZnO.

Sample	Lattice parameter a (Å)	c (Å)	Crystallite size (nm) (D)	Bond Length (Å)	Cell volume (Å^3)	c/a ratio	Band gap (eV)
S0	3.244	5.198	-	1.975	47.37	1.60	3.01
S0.5	3.243	5.196	39.55	1.973	47.32	1.60	2.99
S1	3.236	5.184	37.44	1.969	47.01	1.60	2.94
S2	3.245	5.198	37.30	1.974	47.40	1.60	3.07
S3	3.248	5.202	34.65	1.976	47.52	1.60	3.10

B. Raman Spectroscopy

To study the influence of Cr doping on vibrational modes of zinc oxide, Raman spectra of pure and Cr doped ZnO have been investigated. Figure 2 displays Raman spectrum of pure and Cr doped ZnO in the range 200-800 cm^{-1} at room temperature. The Raman active zone-center optical phonons according to the group theory can be represented as

$$\Gamma opt = A_1+E_1+2E_2 \quad (5)$$

Raman active phonons are categorized as polar and non-polar phonons. The polar phonons comprise of A_1 and E_1 symmetries whereas non-polar phonons have E_2 symmetry. Polar phonons are further of two types depending on their frequencies: transverse (TO) and longitudinal (LO) optical

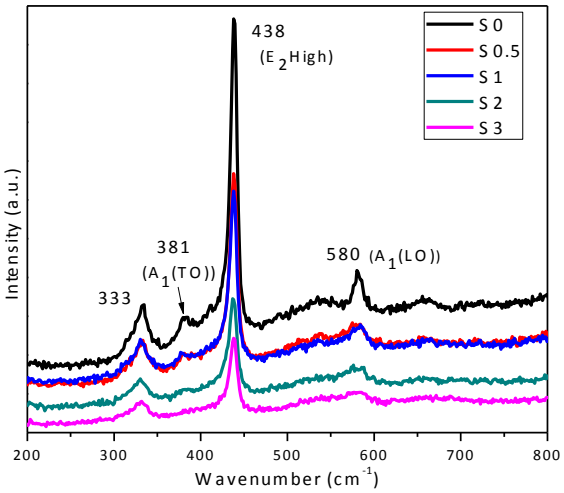

Fig. 2. Raman spectra at room temperature from 200 – 800 cm^{-1} for ZnO (S0) and Cr^{3+}doped ZnO (S0.5, S1, S2, S3).

phonons. The non-polar Raman active modes have two frequencies namely, E_2 (high) and E_2 (low) [25].

Figure 2 indicates the Raman active mode of pure ZnO positioned at 333, 381, 438 and 580 cm^{-1}. The Raman active modes near 381, 438 and 580 cm-1 are associated with the first order phonon spectrum, whereas peak at 333 cm^{-1} is ascribed to the second order phonon spectrum. Raman mode at 381 cm^{-1} corresponds to transverse optical phonon for A_1 symmetry i.e. A_1 (TO). The typical Raman active peak of wurzite crystal structure is the sharp 438 cm^{-1} peak assigned to E_2 (high) mode whereas the peak 580 cm^{-1} corresponds to A_1(LO) [26, 27]. The peak at 438 cm^{-1} is associated to the crystal stress, while the peak at 580 cm^{-1} LO phonon mode corresponds to the defects arising due to oxygen vacancies, zinc interstitial or change of free carrier concentration [28]. When polar semiconductor material possess significant free charge carrier concentration, a coupling between LO phonons and plasmons (Oscillations of the free carriers) may occur resulting in phonon-plasmon interaction. This interaction produces characteristics Raman scattering that provides information on free charge carrier density [29]. From literature it has been found that intensity of A_1 (LO) mode decreases with increase in charge carrier concentration [26]. It is observed from Fig. 2 that all samples have wurzite phase but the peaks become broader and less intense with increase in dopant concentration. Also the intensity of A_1 (LO) mode decreases, which may be attributed to the increase in carrier concentration due to Cr^{3+} doping in zinc oxide lattice. Similar result has been reported by Wang et al. [30]. The shifting in peaks, decrease in the peak intensity and its broadening is attributed to the substitution of zinc ions with chromium ions, creating structural disorder in the lattice [31]. No extra peaks corresponding to Cr_2O_3 phase in the spectra has been observed.

C. X-ray photoelectron spectroscopy

To investigate the elemental composition and oxidation states of pure and chromium doped zinc oxide, XPS measurements were performed. To avoid errors in peak shifts due to charging, all peaks were calibrated considering carbon, C1s (284.6 eV) peak as a reference. High resolution multiplex spectra for Zn, Cr and O corresponding to sample S1 is shown in Fig. 3. The elemental composition determined from XPS studies have been summarized in Table 2. The high resolution spectra obtained for zinc as depicted in Fig 3(a), have binding energies at 1021.6 eV and 1044.69 eV which are associated to $Zn2p_{3/2}$ and $Zn2p_{1/2}$ core levels, respectively [32]. The observed energy difference between two peaks is 23.09 eV which matches well with the standard reference, confirming that zinc is present in Zn^{2+} state. Figure 3(b) represents splitting of Cr 2p level into doublet having different binding energy values. It is evident that Cr $2p_{3/2}$ and $2p_{1/2}$ are located at binding energy 577.05 eV and 587.25 eV respectively confirming the presence of chromium in Cr^{3+} oxidation state. According to the reported data, different values of binding energy for chromium are associated with its various oxidation states such as, Cr metal has B.E at (574.0 eV); Cr^{4+} at 576.3 eV and Cr^{3+} at 577.0–577.2 eV [22]. The O1s peak was Gaussian fitted into three peaks namely O_1, O_2, and O_3. The peak O_1 at B.E 530.17 eV is associated with lattice oxygen bonded to Zn^{2+} and Cr^{3+}. The peak O_2 at B.E. 531.40 eV corresponds to O^{2-} ions in the oxygen deficient regions. The O_3 peak at binding energy 532.07 eV is ascribed to chemisorbed oxygen species on the surface of oxides [33]. Thus, XPS analysis confirms incorporation of chromium in the form as Cr^{3+} in ZnO lattice.

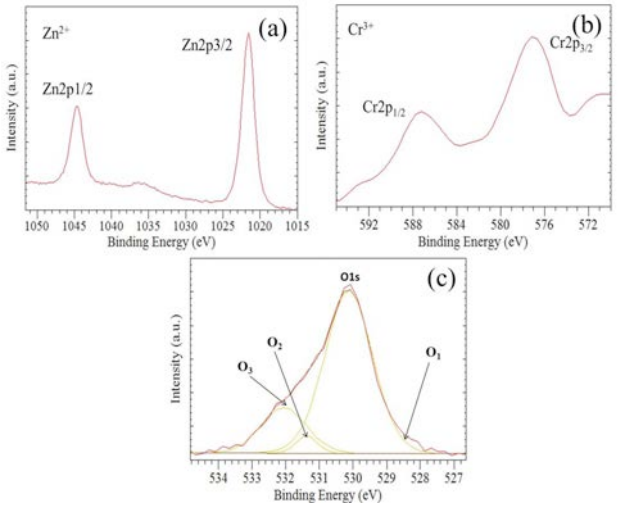

Fig. 3. XPS high resolution spectra of S1 sample.

D. FESEM Analysis

To know the morphology of synthesized samples, FESEM measurements were performed. Fig. 4 represents FESEM micrographs of pure and chromium doped zinc oxide samples. In sample S0, dumbbell shaped microstructures of ZnO of various sizes can be seen in Fig. 4(a). The dumbbell shaped structure is composed of two hexagonal prisms and have dimensions about 6-7 micron in length and 2-3 micron in diameter. In sample S0.5, there is a formation of few spherical particles on surface of ZnO micro rods and the dumbbell

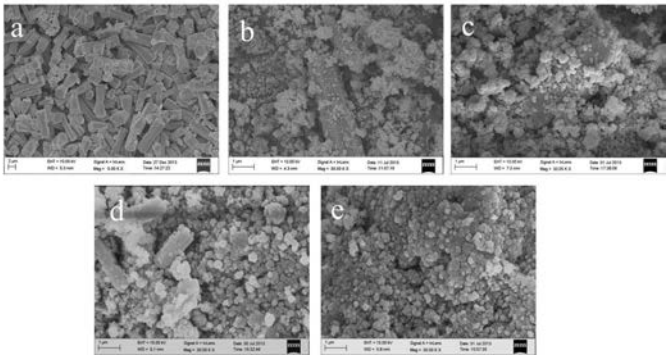

Fig. 4. FESEM micrographs of (a) S0 (b) S0.5 (c) S1 (d) S2 (e) S3.

shape is vanished as shown in Fig. 4(b). As doping is increased for sample S1, micro rods of ZnO start diminishing in size whereas population of spherical particles starts increasing around the surface of ZnO microrods, as shown in Fig. 4(c). With further increase in concentration of chromium upto 3 wt. %, rod like structures completely vanish, and only spherical particles are visible which are well agglomerated.

The incorporation of chromium into ZnO has a significant influence on the nucleation and growth processes that brought about alteration in morphology. The nucleation and growth process can be explained on the basis of change in surface energy. Surface energy of the solid nucleus during synthesis is influenced by many factors such as temperature, use of different solvents, additives in solutions and incorporation of impurities into solid phase [34]. With addition of Cr as a dopant in ZnO, the surface energy of solid nucleus increases. This energy increase appears at the expense of reduction in Gibb's free energy favouring high supersaturation. At high supersaturation, crystal nucleation dominates crystal growth, resulting in large number of small sized nuclei which means reduction in grain size (also according to XRD results).

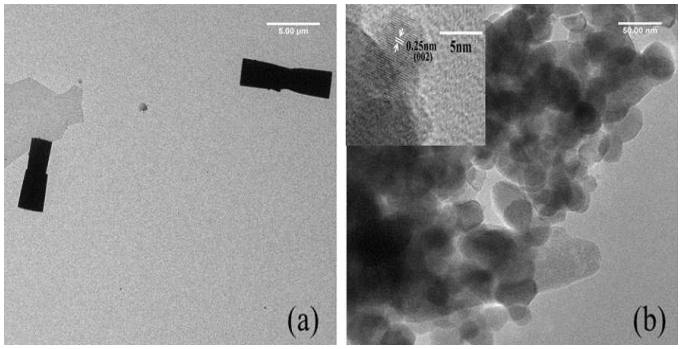

Fig. 5. TEM micrographs of S0 and S1 sample.

E. TEM

The TEM micrographs of pure and 1wt. % Cr doped ZnO are shown in Fig.5. For pure zinc oxide (Fig.5(a)), dumbbell shaped rods having dimensions 6-8 μm in length and 2-3 μm in diameter are observed whereas for 1wt. % Cr dopant, the dumbbell shape no more exists and a rod like structure covered with large number of spherical shaped particles ranging in 27-48 nm is clearly visible. The morphology observed from TEM micrographs, agrees well with FESEM images. The inset of Fig. 5(b) shows HRTEM image of spherical nanoparticle, resting on the surface of a rod. The calculated interplanar spacing 'd' is 0.25 nm corresponding to (002) plane of ZnO.

F. Optical Properties

Using UV-Visible absorption spectroscopy at room temperature, optical absorption spectra for pure and Cr doped zinc oxide samples were obtained. The mechanism that works in this technique is the excitation of electrons from valence to conduction band when a photon lying in UV-Vis range is incident on it. Therefore band gap is the energy required to excite an electron from maxima of valence to minima of conduction band. Fig. 6 represents plot between absorbance and wavelength for samples S0 to S3. Band gap energies were calculated from Tauc's plot by using the relation

$$\alpha h \quad = A\,(h \quad - E_g)^n \qquad (6)$$

where α is the absorption coefficient, h is the photon energy, n = 1/2 or 2 for direct and indirect transitions, respectively, and E_g is the optical band gap. Figure 6 shows optical band gap spectra for pure and Cr doped zinc oxide. Extrapolation of linear region of the graph between $(\alpha h\nu)^2$ and photon energy $h\nu$ gives the value of band gap energy

E_g. The values of band gap energy for each sample are given in Table 1.

TABLE II
SURFACE ELEMENTAL COMPOSITION (% ATOMIC CONCENTRATION) OF S0 (PURE), S1 (1WT. %) AND S3 (3WT. %) CR DOPED ZNO

Elements	%Atomic concentration		
	S0	S1	S3
Zn	36.7	42.82	38.82
O	63.7	56.24	58.26
Cr	-	0.94	2.91

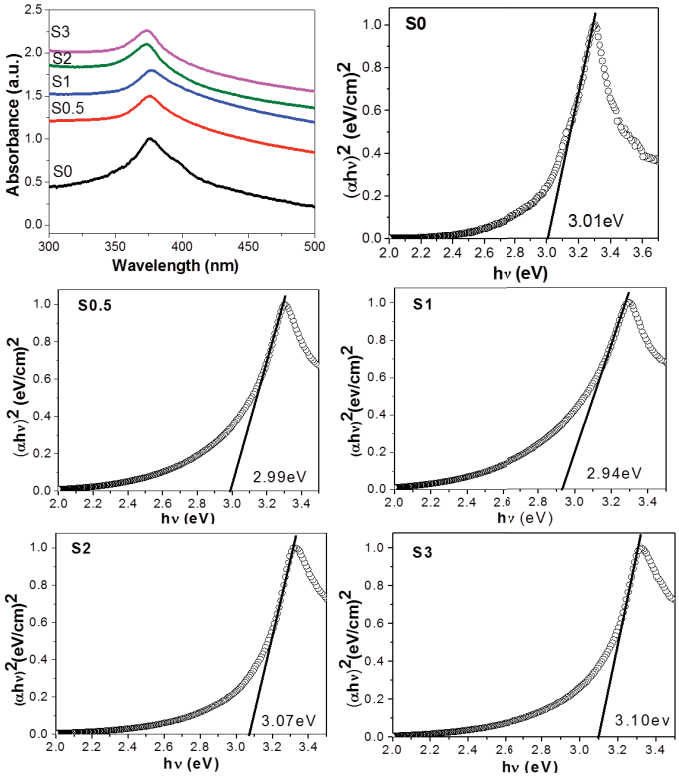

Fig. 6. Absorption spectra of ZnO and Cr^{3+} doped ZnO and $(\alpha h\upsilon)^2$ vs photon energy ($h\upsilon$) plots for determination of band gap energies.

From the table it is clear that band gap energies for samples S0.5 and S1 have smaller values as compared to S0 whereas for samples S2 and S3 these energies are comparable with that of S0. The decrease in optical band gap for sample S0.5 and S1 can be explained on the basis of sp-d spin exchange interaction between band electrons and the localized d electrons of doped transition metal ions. The 3d orbitals of doped chromium atom can split and interfere with conduction band and valence band, creating impurity energy level and therefore resulting in redshift of absorption band. However with increase in dopant concentration, a widening in band gap is observed which can be related to Burstein Moss effect [35].

G. *Sensing response*

The fabricated pure and Cr^{3+} doped zinc oxide based sensors were exposed to 250 ppm of LPG, at various temperatures in order to determine the optimum operable temperature as shown in Fig. 7. From these plots, the optimum operable temperature for pure and chromium doped zinc oxide gas sensor were found to be 400 and 300°C, respectively. The chromium doping in zinc oxide resulted in reduction of optimum operable temperature from 400 to 300°C. The catalytic nature and lower ionization energy of chromium as compared to zinc caused reduction of activation energy of the reaction between target gas molecules and surface adsorbed oxygen which leads to fall in operating temperature of zinc oxide gas sensor. The low is the ionization energy, the less is energy required to knock out electron which leads to reduction in activation energy of chemisorption of gases [18]. The lowering of activation energy due to catalytic effect can take place by two possible mechanisms. First, it can concentrate the reactants by adsorption, thus increasing their probability of interacting. Second, it can introduce a reaction route of very low activation energy [34].

The trend in sensing response towards LPG for pure and doped samples as depicted in Fig. 7 varies in the order as follows: S1 > S0.5 > S2 > S3> S0. The rapid increase and gradual decrease in LPG sensing response with varying dopant concentration in ZnO can be explained with increase in charge carrier concentration due to incorporation of Cr^{3+} at substitutional and interstitial sites. The presence of Cr^{3+} atoms at substitutional site or interstitial site in ZnO lattice depends on the concentration of dopant atom. As is evident from XRD results, Zn^{2+} is substituted by Cr^{3+} till 1 wt. % doping and above 1 wt. %, Cr^{3+} is positioned at interstitial sites. The incorporation of Cr^{3+} atoms at substitutional sites in ZnO lattice creates an extra free electron while Cr^{3+} occupying interstitial position creates three free electrons (Fig.8). Increase in charge carrier concentration with increase in chromium content is also supported by Raman and optical studies. Larger is the charge carrier concentration; the wider will be the depletion region due to higher oxygen adsorption on sensor surface. Therefore an increase in sensing response towards LPG as compared to pure zinc oxide (S0) is observed in case of S0.5 and S1. The gradual decrease in sensing response above 1wt. % could be explained as follows:

The presence of Cr^{3+} at substitutional and interstitial sites act as charge defects in ZnO lattice and causes ionized impurity scattering of electrons. Ionized impurity scattering occurs in doped materials. The reason for ionized scattering is existence of coulomb interaction between ionized donor /acceptor impurities and charge carriers (electrons and holes).

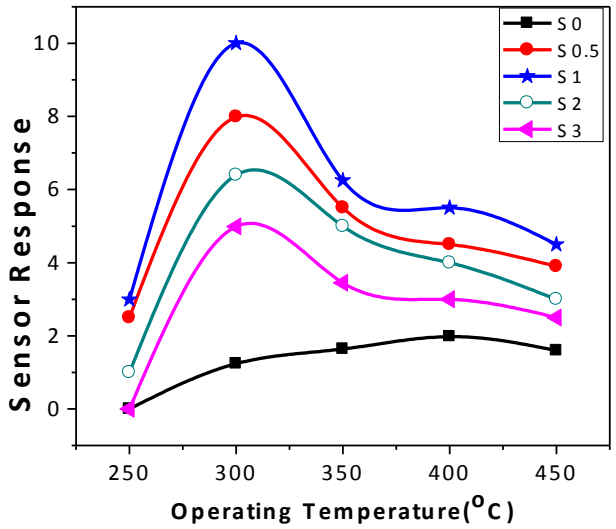

Fig. 7. Sensor response as a function of operating temperature on exposure to 250 ppm of LPG.

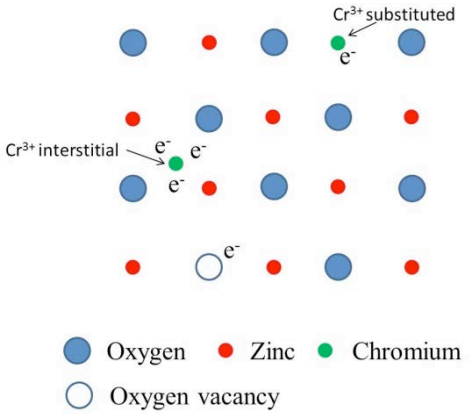

Fig. 8. Schematic diagram for interstitial and substitutional doping of Cr^{3+} in ZnO lattice.

These coulomb interactions result in scattering of charge carriers when they approach the vicinity of ionized impurity atom [9]. Therefore, higher is the dopant concentration more is ionized impurity scattering from substiutional and interstitial dopant sites resulting in reduction of mean free path of electrons. Hence the decrease in sensor response at higher doping for S2 and S3 could be because of two reasons; firstly due to decrease in mobility of charge carriers because of augmented scattering from ionized impurity atoms and secondly because of dopant segregation at grain boundaries preventing diffusion of oxygen into the bulk [36].

Further sensing investigations were performed on sample S1 at optimum operable temperature of 300°C. Fig. 9 represents sensor response versus time for S1 and S0 sample towards 250 ppm LPG at an operating temperature of 300°C and 400°C. The sensor exhibits a maximum response (Ra/Rg) of magnitude 10 with a response time of 22 sec and a recovery

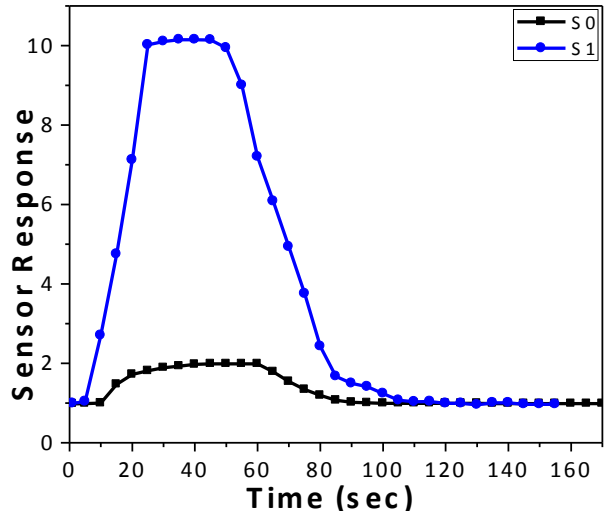

Fig. 9. LPG sensor response versus time curve for S0 and S1 sensor.

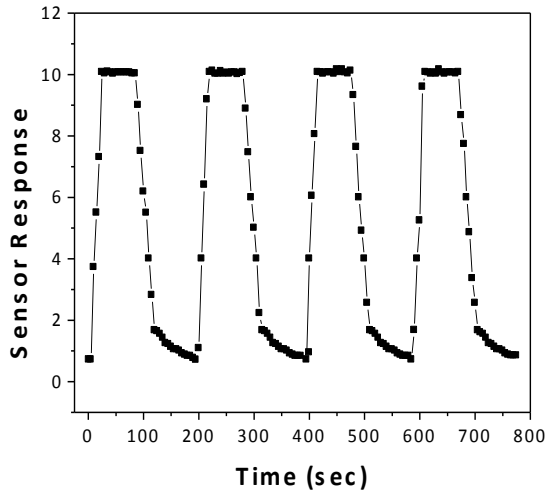

Fig. 10. Sensor response of S1 sensor on repeated exposure to 250 ppm LPG.

time of 40 sec. Besides sensitivity, stability and reproducibility are also important characteristics for a gas sensor. The sensing performance of S1 sensor towards 250 ppm LPG was repeated at regular time intervals and results are shown in Fig 10. It is clear from Fig. 10 that sensor response profile is repetitive indicating that sensing response is stable and reproducible. Sensor response of sensor S1 towards acetone, ethanol and LPG is depicted in Fig 11. An interesting observation inferred from Fig. 11 is that Cr doping has slightly improved the sensing response towards ethanol and acetone whereas for LPG, sensing response has significantly improved (5 times) as compared to pure zinc oxide. It is challenging to explain the sensing response variation towards different gases but still there are some facts that might explain the variation in sensor response. One of the possible reasons could be catalytic behavior of chromium towards LPG that has lowered activation energy, favoring the reaction between absorbed

O_2 and injected LPG over other gas species. Another plausible

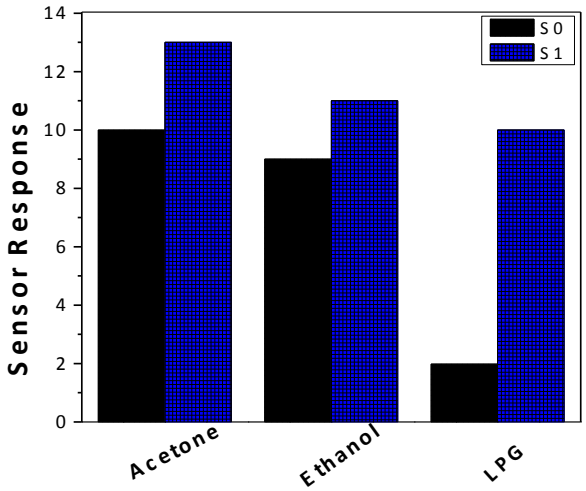

Fig. 11. Histogram depicting sensor response of S0 and S1 towards acetone, ethanol and LPG.

reason for high sensing response towards LPG as compared to ethanol and acetone is oxidation of the target gases through the following complex series of reactions, thereby consuming 6, 8 and 13 O^- (ads) by ethanol, acetone and LPG respectively. Similar results have been reported by Gong et al. [37].

$$C_2H_5OH+6O^- \rightarrow 3H_2O+2CO_2+6e- \quad (7)$$
$$C_3H_6O+8O^- \rightarrow 3\,CO_2+3H_2O+8e- \quad (8)$$
$$C_4H_{10}+13O^- \rightarrow 5H_2O+4CO_2+13e- \quad (9)$$

The decrease in resistance of synthesized samples on exposure to LPG confirms their n-type behaviour. When metal oxide sensor surface is exposed to air, oxygen molecules adsorb on surface of the material forming O^{2-}, O^-, O_2^- ions by capturing electrons from the conduction band. This results in high sensor resistance in air.

$$O_2\,(gas) \rightarrow O_2\,(ads) \quad (10)$$
$$O_2\,(ads) + e^- \rightarrow O_2\text{-}\,(ads) \quad (11)$$
$$O_2\,(ads) + 2e^- \rightarrow 2O^-\,(ads) \quad (12)$$

On exposure of metal oxide sensors to LPG, the gas molecules react with adsorbed oxygen and as a result release captured electrons to conduction band as:

$$C_4H_{10}\,(gas) +13O^- \rightarrow 4\,CO_2\,(gas) +5\,H_2O\,(gas) +13\,e- \quad (13)$$

These electrons increase the conductivity of metal oxide based sensors.

IV. CONCLUSION

Chromium doped zinc oxide particles were successfully synthesized by co-precipitation route. XRD results reveal the presence of hexagonal wurtzite structure of pure and Cr doped ZnO samples. Variation in lattice constants and unit volume confirms the incorporation of chromium into ZnO lattice at substitutional and interstitial sites. The decrease in intensity of A1 (LO) Raman active modes signifies the increase in charge carrier concentration due to Cr^{3+} dopant in zinc oxide. XPS investigations assisted in determination of elemental compositions and presence of chromium as Cr^{3+} in ZnO lattice. With addition of dopant, the optimum operable temperature of zinc oxide sensor has reduced from 400°C to 300°C. Chromium doped ZnO samples have selectively enhanced the LPG response as compared to ethanol and acetone. A concentration of 1 wt. % Cr^{3+} doped ZnO gives maximum sensing response for LPG in comparison to other concentrations. This is attributed to the increase in charge carrier concentration, catalytic effect of Cr^{3+} and lattice disorder.

ACKNOWLEDGMENT

One of the authors Ms. Anita Hastir would like to thanks Department of Science & Technology for awarding INSPIRE Fellowship. We would like to thanks UGC-UPE and DST-FIST for providing instrumental facilities and Bhai Gurdas library, GNDU for providing access to Urkund software for plagiarism check. We would also like to thanks Prof. Robert L. Opila at University of Delaware for his help with XPS instrument.

REFERENCES

[1] A. Rothschild, Y. Komem, “The effect of grain size on the sensitivity of nanocrystalline metal-oxide gas sensors,” *J. Appl. Phys.*, vol. 95, pp. 6374-6380, 2004.
[2] W. S. Lee, G. W. Choi, Y. J. Seo, “Surface planarization of ZnO thin film for optoelectronic applications,” *Microelectron.*, vol. 40, pp. 299–302, 2009.
[3] I. Concina, A. Vomiero, “Metal Oxide Semiconductors for Dye- and Quantum-Dot-Sensitized Solar Cells,” *small*, vol 11, pp. 1737-1856.
[4] O. Singh, R. C. Singh, “The Enhancement in ethanol sensing response by surface activation of ZnO with SnO2,” *Materials Research Bulletin.*, vol. 47, pp. 557–561, 2012.
[5] A. M. Willander, O. Nur, Q. X. Zhao, L.L. Yang, M. Lorenz, B.Q. Cao, J. Z. Perez, C.Czelalla, G. Zimmermann, M. Grundmann, A. Bakin, A. Behrends, M. A. Suleiman, A.E. Shaer, A. C. Mofor, B. Postels, A. Waag, N. Boukos, A. Travlos, H.S. Kwack, J. Guinard and D.L.S. Dang, “Zinc oxide nanorod based photonic devices: recent progress in growth, light emitting diodes and lasers sensors,” *Nanotechnology.*, vol. 19, 2009
[6] R. Kumar, O. A. Dossary, G. Kumar, A. Umar, “Zinc Oxide Nanostructures for NO2 Gas–Sensor Applications: A Review”, *Nano-Micro Lett.* vol. 7(2), pp. 97–120, 2015
[7] O. Singh, N. Kohli, R. C. Singh, “Precursor controlled morphology of zinc oxide and its sensing behavior”, *Sens. and Actuators B.* vol. 178, pp. 149– 154, 2013.
[8] S. Pati, P. Banerji, S. B. Majumder, “Properties of indium doped nanocrystalline ZnO thin films and their enhanced gas sensing performance” *RSC Adv.*,vol 5,pp. 61230, 2015.
[9] A K. Galatsisa, L. Cukrovb , W. Wlodarskia , P. M. Cormickb , K. K. Zadeha , E. Cominic , G. Sberveglieric, “p- and n-type Fe-doped SnO2 gas sensors fabricated by the mechanochemical processing technique”, *Sens. and Actuators B*, vol 93, pp.562–565, 2003.
[10] M. Batzill, U. Diebold, “The surface and materials science of tin oxide”, *Progress in Surface Science.*, vol 79,pp. 47–154, 2015.
[11] M. S. Berberich, J.G. Zheng, U. Weimer, W. Gopel, N. Barsan, E. Pentia, A. Tomescu, “The effect of Pt and Pd surface doping on the response of nanocrystalline tin oxide gas sensors to Co,” *J Sens. Actuators B.*, vol. 1-2, pp. 71-75, 1996.
[12] G. Korotcenkov, I. Boris, V. Brinzari, S.Han, B .K. Cho, “The role of doping effect on the response of SnO2-based thin film gas sensors:

analysis based on the results obtained for Co-doped SnO2 films deposited by spary pyrolysis," *J. Sensors and Actuators.*, vol. 93, pp. 562–565, 2003.

[13] X. H. Zhang, J. Chen , Y. Wu, Z. Xie, J. Kang, L. Zheng, "A simple route to fabricate high sensibility gas sensor based on erbium doped ZnO nanocrystal, colloids and surfaces" *Physicochem. Eng.Aspects* vol. 384,pp. 580-584, 2011.

[14] Junjie Qi, Hong Zhang, Shengnan Lu,Xin Li, Minxuan Xu, Yue Zhang, "High Performance Indium-Doped ZnO Gas Sensor", *Journal of Nanomaterials*,,pp. 954747, 2015.

[15] K. M. Kim, H.M. Jeong, H.R. Kim, K. Choi, H. J. Kim and J. H. Lee, "Selective Detection of NO2 Using Cr-Doped CuO Nanorods" *Sensors*, vol 12, 2012.

[16] X. Sun, X. Hu, Y. Wang, R. Xiong, X. Li, J. Liu, H. Ji, X. Li, S. Cai, and C. Zheng "Enhanced Gas-Sensing Performance of Fe-Doped Ordered Mesoporous NiO with Long-Range Periodicity" *J. Phys. Chem.* C, vol 119 (6), pp 3228–3237, 2015.

[17] D.R.Patil,L.A.Patil, "Cr2O3-modified ZnO thick film resistors as LPG sensors", *Talanta*, vol 77, pp. 1409-1414, 2009.

[18] N.H. Al-Hardan, M.J.Abudullah, A. Abdul Aziz, "Performance of Cr-doped ZnO for acetone sensing" *Applied Surface Science*, vol 270,pp. 480-485, 2013

[19] D. Mihajlov,A. Andreev, "Spectral and Catalytic properties of a chromium containing polymeric complex" *Reaction Kinetics and Catalysis Letters*, Vol. 8, pp. 521-526, 1978.

[20] V. Talwar, O. Singh, R. C. Singh, "ZnO assisted polyaniline nanofibers and its application as ammonia gas sensor" *Sensors and Actuators B*, vol 191,pp. 276– 282, 2014.

[21] A. Fouchet, W. Prellier, P. Padhan, Ch. Simon, B. Mercey, V. N. Kulkarni, T. Venkatesan, "Structural and magnetic properties of a series of low-doped $Zn_{1-x}Co_xO$ thin films deposited from Zn and Co metal targets on (0001) Al2O3 substrates,"*J.Appl. Phys*. Vol 95, pp. 7187 2004.

[22] Y. C. Yang, C. Song, X. H. Wang, F. Zeng, F. Pan, "Cr-substitution-induced ferroelectric and improved piezoelectric properties of Zn1−xCrxO films "*J. Appl. Phys*., vol 103,pp. 074107, 2008.

[23] J. Hays, A. Punnoose, R. Baldner, M. H. Engelhard, J. Peloquin, K. M. Reddy, "Relationship between the structural and magnetic properties of Co-doped SnO2 nanoparticles," *Phys. Rev B*,vol 72,pp. 075203, 2005.

[24] V. Gandhi, R. Ganesan, H. H. A. Syedahamed, and M. Thaiyan, "Effect of cobalt doping on structural, optical and magnetic properties of ZnO Nanoparticles Synthesized by coprecipitation method" *The journal of Physical Chemistry C*, vol 118, pp. 9715-9725, 2014

[25] R. Bhargava, P.K. Sharma, S.Kumar, A.C. Pandey, N.Kumar, "Consequence of doping mediated strain and the activation energy on the structural and optical properties of ZnO:Cr nanoparticles," *J. Solid State Chem*, vol 183,pp. 1400-1408, 2010

[26] X. Wanga, S. Yanga, J. Wanga, M. Lia, X. Jianga, G. Dua, X. Liub, R.P.H. Chang, "Nitrogen doped ZnO film grown by the plasma-assisted metal-organic chemical vapor deposition" *Journal of Crystal Growth*, vol 226,pp. 123–129, 2001

[27] A. Alim, V. A. Fonoberov, M. Shamsa, A. A. Balandin, "Micro Raman investigation of optical phonons in ZnO nanocrystals," *J.Appl.Phys*. vol 97, pp.124313, 2005

[28] B. Cheng, W. Sun, J. Jiao, B. Tian, Y. Xiao and S. Lei, "Disorder-induced Raman scattering effects in one-dimensional ZnO nanostructures by incorporation and anisotropic distribution of Dy and Li codopants" J. Raman Spectrosc.,vol, 41, pp.1221–1226,2010

[29] W.H.Weber and R.Merlin, " Raman Scattering spectroscopy and Analyses of III-V nitrides-based materials in Raman Scattering in Material Science, 1st ed, Springer-verlag Berlin Heidelberg, New York in 2000.

[30] S. Wang, M. Zhong, C. Liu, Y. Li, M. Zhu, H. Jin, and Y. Hu, "Effects of Temperature on the Microstructure and Magnetic Property of Cr-Doped ZnO DMS Prepared by Hydrothermal Route Assisted by Pulsed Magnetic Fields" Volume 2013, Article ID 830372, 7 pages

[31] R.S. Zeferino, U. Pal, R. Melendrez, H.A.D. Munoz, M.B. Flores, "Dose enhancing behavior of hydrothermally grown Eu-doped SnO2 nanoparticles" *J. Appl. Phys*. vol 113,),pp. 064306, 2012.

[32] J.F.Moulder, W.F. Strickle, P.E. Sobol, K.D. Bomben, Handbook of X-ray Photoelectron Spectroscopy, ULVAC-PHI, Inc.,370 Enzo, Chigasaki,1995.

[33] Y.C. Liang, H.Y. Hsia, Y.R. Cheng, C.M. Lee, S.L. Liu, T. Yin and C.C. Chung, "Crystalline quality-dependent gas detection behaviors of zinc oxide–zinc chromite p–n heterostructures", *Cryst Eng Comm*, vol 17,pp. 4190-4199, 2015.

[34] G. Cao, "Synthesis, Properties & Applications" in Nanostructures and Nanomaterial,1st ed., Imperial College Press, London, 2004.

[35] B. Choudhury, A. Choudhury, "Lattice distortion and corresponding changes in optical properties of CeO_2 nanoparticles on Nd doping",vol 13,pp.217-223, 2013.

[36] J. Ma, F. Ji, H.l. Ma, S.Y. Li, "Preparation and properties of transparent conducting zinc oxide and aluminum-doped zinc oxide films prepared by evaporating method", *Solar Energy Materials & Solar Cells*, vol 60, pp.341-348, 2000.

[37] H. Gong, Y.J. Wang, S.C. Teo, L. Huang, Interaction between thin-film tin oxide gas sensor and five organic vapors, *Sens. Actuators B*,vol 54 pp.232–235, 1999.